## Supporting Information

Analysis of the X-ray powder diffraction data proceeded in the usual sequence of steps:

1. Data Collection
2. Indexing the Pattern
3. Extraction of the Peak Intensities
4. Structure Determination
5. Rietveld Refinement

The results are reported in the main manuscript. Further information regarding the details of the analysis and choices made along the way are given in the material that follows.

### ***1. Data Collection***

*$Mo_4OXA$*

X-ray powder diffraction data were initially collected at the X7A beamline of the National Synchrotron Light Source (NSLS) at Brookhaven National Laboratory (BNL) on sample of $[(^tBuCO_2)_3Mo_2(\mu\text{-}O_2C_2O_2)Mo_2(O_2C^tBu)_3]$ ($Mo_4OXA$) and the tungsten analogue ($W_4OXA$) sealed in 0.7 mm diameter capillaries. Data were collected over the angular range 4-45º 2θ at a wavelength of 0.8000 Å using a linear position sensitive detector (PSD). The $Mo_4OXA$ and $W_4OXA$ diffraction patterns were very similar in both the positions and intensities of the peaks, strongly suggesting that these two compounds are isostructural. Unfortunately, the peaks in the $W_4OXA$ pattern broadened and became weak fairly rapidly as a function of 2θ, suggesting considerable strain and disorder. For this reason the $W_4OXA$ pattern was not suited for detailed structural analysis.

Attempts to obtain a unit cell for $Mo_4OXA$ from the initial synchrotron X-ray powder diffraction pattern were not successful. In retrospect this failure can be attributed to two factors: (a) the experimental setup (λ = 0.8000 Å, detector = PSD) did not allow us to collect data below 4º 2θ, so that the first three reflections were not observed, and (b) the sample showed some signs of oxidation, as indicated by its brown color. Our second round of data collection was carried out on a fresh sample using an in-house Bruker D8 diffractometer. This system is equipped with a Cu X-ray tube, an incident beam Ge monochromator, a spinning capillary stage, and a scintillation detector. This time we noted that the red coloration of the sample did not change during the course of data collection, and we were able to observed the three low angle peaks missing from the synchrotron pattern. Inclusion of these peaks allows us to index the pattern as described in the next section.

Once the unit cell had been determined we elected to load a 0.5 mm diameter capillary with fresh sample and collect additional data at the NSLS in hopes of taking advantage of the high-resolution and low signal-to-noise capabilities of the X7A diffractometer. Two data sets were collected on this third sample. The first pattern was obtained over the 2θ range 1-22º, using a wavelength of 1.1983 Å, a Ge 220 analyzer crystal in the diffracted beam and a scintillation detector. This data set was very similar to the pattern collected on the Bruker D8 system, confirming that both samples corresponded to the same phase. The second data set was obtained over the 2θ range 3.75 – 35.75º, using a wavelength of 0.70187 Å, and the linear PSD. Due to the excellent signal-to-noise ratio that can be obtained by using a synchrotron source and a PSD in combination, as well as the high quality of this sample, this data set contained more resolved

reflections than any of the previous patterns. However, as before the first three reflections were not included in the measured data range. Subsequent data analysis was carried out using either this final synchrotron data set, the laboratory data set, or both as described below.

*$Mo_4PFT$*

X-ray powder diffraction data were collected on fresh samples of $[(^tBuCO_2)_3Mo_2(\mu\text{-}O_2CC_6F_4CO_2)Mo_2(O_2C^tBu)_3]$ ($Mo_4PFT$) and the tungsten analogue ($W_4PFT$) using the in-house Bruker D8 diffractometer described above. In a similar fashion to the oxalate complexes, the $Mo_4PFT$ and $W_4PFT$ diffraction patterns were very similar in both the positions and intensities of the peaks, suggesting that these two compounds are isostructural, although the XRD pattern of the tungsten compound were not of sufficient quality to warrant further analysis.

## ***2. Indexing the Pattern***

The positions of the first 16 peaks for $Mo_4OXA$ and 18 peaks for $Mo_4PFT$ in the laboratory diffraction patterns were determined using the peak fitting routine in DASH.[1,2] The peak positions were then input to the autoindexing program DICVOL-91.[3] At this point the analysis of the two compounds diverged, therefore, they will be discussed separately below.

*$Mo_4OXA$*

A number of promising solutions were obtained, but further inspection revealed that some solutions were simply different settings of the same monoclinic space group. Once this was recognized two independent solutions emerged:

Unit Cell **A**: a = 30.36 Å, b = 5.93 Å, c = 13.43 Å, β = 111.86° [F = 63]
Unit Cell **B**: a = 26.87 Å, b = 5.83 Å, c = 16.10 Å, β = 118.77° [F = 48]

Solution **A** gives a somewhat higher figure of merit[4], but both solutions account for all of the observed reflections. Therefore, neither solution was discounted at this point. Our next task was to determine the correct space group symmetry. With unit cell **A** no clear systematic absences beyond a $2_1$ screw axis could be found. However, indexing with unit cell **A** and space group $P2_1$ leaves a considerable number of "accidentally absent" peaks. If unit cell **B** is used to index the unit cell, the systematic absences suggest the presence of either an *a*-glide plane or C-centering. Due to the small value of the *b*-axis, and the presence of some peak overlap it is not straightforward to distinguish between the two symmetry elements, nor to unequivocally confirm the presence of a $2_1$ screw axis. The observation that the pattern can be indexed with very few accidental absences using unit cell **B**, suggests that it is a more appropriate choice.

*$Mo_4PFT$*

Unlike $Mo_4OXA$ attempts at autoindexing the $Mo_4PFT$ pattern, using both DICVOL[3] and TREOR[5], returned only one unit cell that could account for all of the observed peaks. The unit cell was monoclinic with dimensions a = 21.02 Å, b = 5.72 Å, c = 20.55 Å and β = 101.4°, with a figure of merit $F_{18}$ equal to 34. The systematic absences were consistent with a C-centered unit cell. Further absences, such as those that arise from the presence of an axial glide plane, were not consistent with the data. Thus we were able to narrow the list of possible space groups down to three: *C2*, *Cm* and *C2/m.*

## *3. Extraction of the Peak Intensities*

Peak intensities were extracted using the whole pattern fitting routine in DASH, which is based on the Pawley method,[6] The patterns were also fit using a whole pattern approach based upon the LeBail method[7] as implemented in the GSAS software suite.[8]

*$Mo_4OXA$*

Tables 1 and 2 list the results for the most promising combinations of unit cell dimensions and space group symmetry for the $Mo_4OXA$ patterns, while the LeBail fits to the laboratory and synchrotron data are shown in Figures 1 and 2. The goodness of fit values mirror the results from the autoindexing process, with unit cell A providing a slightly better fit to the experimental patterns. Thus we were not able to uniquely determine the space group prior to the structure solution stage. However, as shown by the arrow in the bottom panel of Figure 2 all of the peaks in the synchrotron data set cannot be accounted for using space group C2 (and thus C2/m), which allowed us to eliminate this space group from consideration. This distinction could not be made using the laboratory data, due to the more rapid decrease in peak intensity as a function of 2θ.

**Table 1:** Possible unit cells for $[(^tBuCO_2)_3Mo_2(\mu\text{-}O_2C_2O_2)Mo_2(O_2C^tBu)_3]$ as determined from the analysis of the monochromatic laboratory X-ray data using DASH. Lattice parameters were recorded following the Pawley fit to the diffraction pattern.

| Space Group | *a* (Å) | *b* (Å) | *c* (Å) | β (°) | Volume (Å$^3$) | Pawley $\chi^2$ | Profile $\chi^2$ |
|---|---|---|---|---|---|---|---|
| $P2_1$ | 28.23 | 5.928 | 13.43 | 94.25 | 2243 | 2.4 | 18.0 |
| C2 | 26.83 | 5.816 | 16.08 | 118.86 | 2198 | 3.5 | 20.3 |
| $P2_1/n$ | 26.87 | 5.826 | 16.09 | 97.59 | 2206 | 3.5 | 11.7 |
| Pa | 26.87 | 5.826 | 16.10 | 97.59 | 2206 | 3.5 | 9.7 |

**Table 2:** Possible unit cells for $[(^tBuCO_2)_3Mo_2(\mu\text{-}O_2C_2O_2)Mo_2(O_2C^tBu)_3]$ as determined from simultaneous analysis of the monochromatic laboratory and synchrotron X-ray data using GSAS. Lattice parameters were recorded following the LeBail fits to the diffraction patterns. The symbols (L) and (S) refer to the Laboratory and Synchrotron data, respectively.

| Space Group | *a* (Å) | *b* (Å) | *c* (Å) | β (º) | Volume (Å$^3$) | LeBail $R_{wp}$ | Rigid Body $R_{wp}$ |
|---|---|---|---|---|---|---|---|
| $P2_1$ | 28.267(3) | 5.9263(5) | 13.434(1) | 94.276(5) | 2244.3(4) | 0.0585 (L)<br>0.0386 (S) | ---<br>--- |
| C2 | 26.842(3) | 5.8173(6) | 16.072(2) | 118.847(7) | 2198.2(6) | 0.0684 (L)<br>0.0480 (S) | ---<br>--- |
| $P2_1/a$ | 26.841(3) | 5.8160(6) | 16.072(2) | 118.866(7) | 2197.2(5) | 0.0662 (L)<br>0.0465 (S) | 0.1534 (L)<br>0.1284 (S) |
| Pa | 26.817(2) | 5.8170(6) | 16.045(2) | 118.826(7) | 2192.7(5) | 0.0708 (L)<br>0.0445 (S) | 0.1056 (L)<br>0.1131 (S) |

**Figure 1:** LeBail fits to the laboratory X-ray powder diffraction data for [($^t$BuCO$_2$)$_3$Mo$_2$(μ-O$_2$C$_2$O$_2$)Mo$_2$(O$_2$C$^t$Bu)$_3$]. Blue points represent the experimental diffraction pattern, the green line represents the refined fit to the pattern, the red line represents the difference curve, and the black ticks mark the expected peak positions.

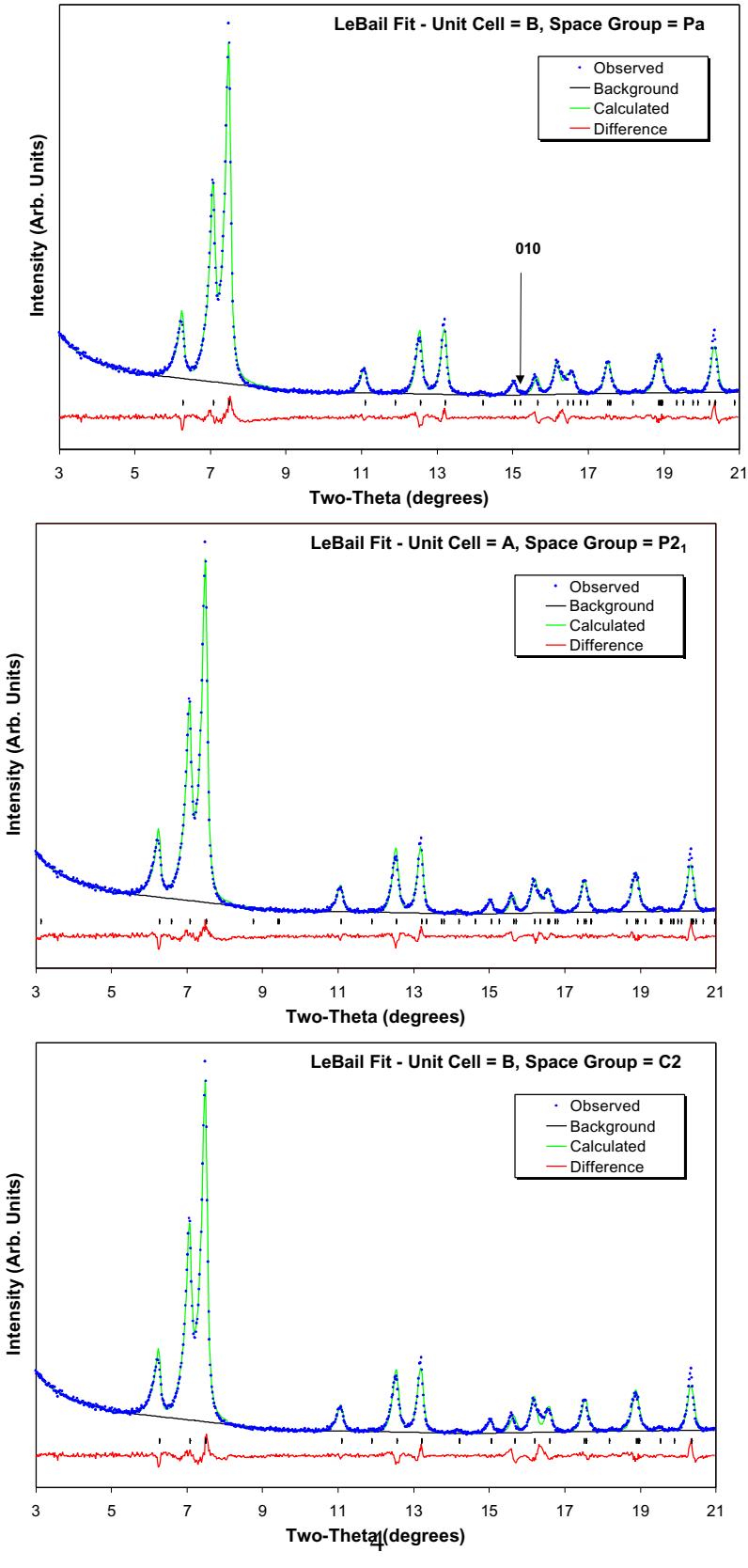

**Figure 2:** LeBail fits to the synchrotron X-ray powder diffraction data for [($^t$BuCO$_2$)$_3$Mo$_2$(μ-O$_2$C$_2$O$_2$)Mo$_2$(O$_2$C$^t$Bu)$_3$]. Blue points represent the experimental diffraction pattern, the green line represents the refined fit to the pattern, the red line represents the difference curve, and the black ticks mark the expected peak positions.

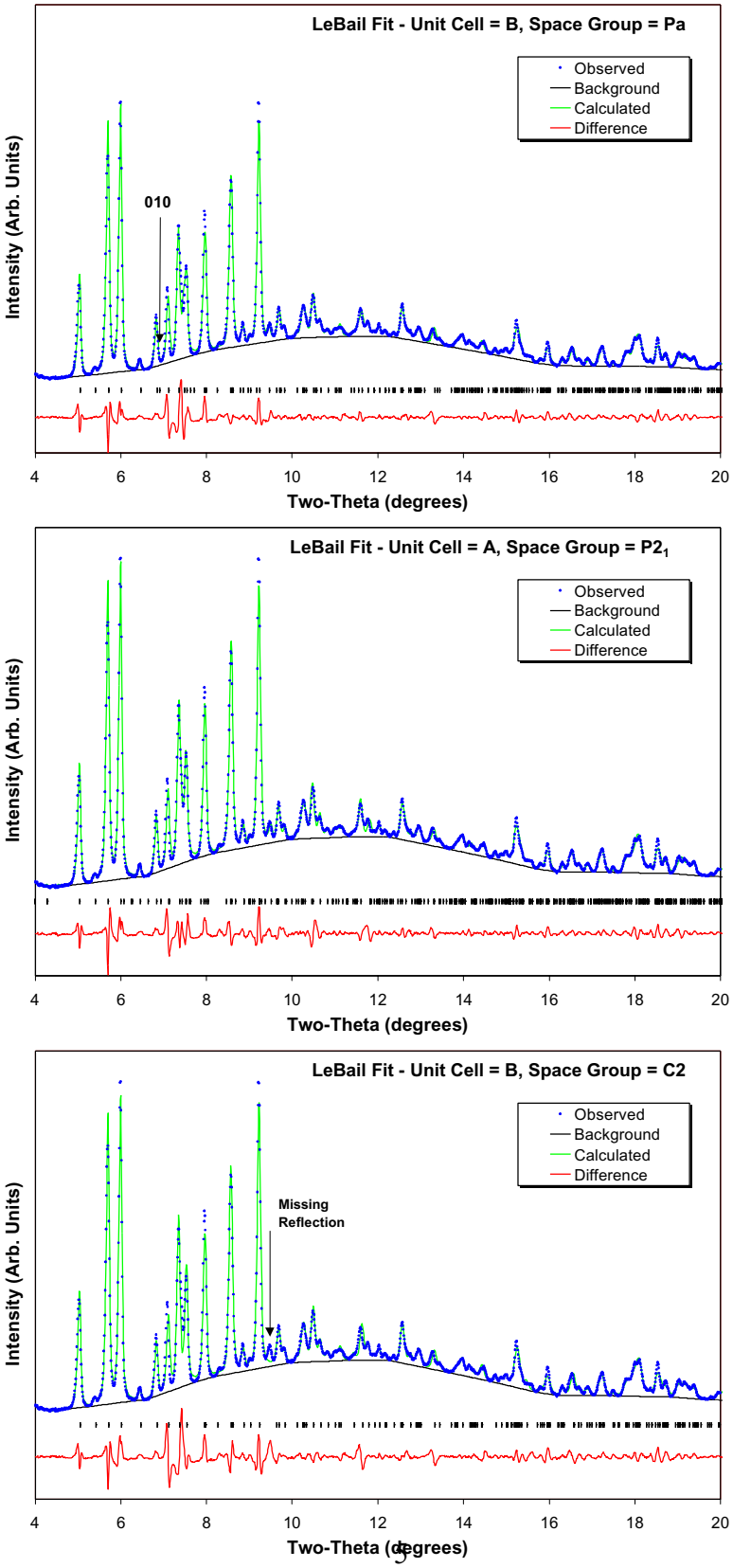

*$Mo_4PFT$*

For $Mo_4$PFT the three space groups that emerged from the indexing stage (*C2, Cm* and *C2/m*) have identical systematic absences so that they all give identical fits to the data at the whole pattern fitting stage. Peak extraction using DASH (Pawley method) gave a profile $\chi^2$ value of 2.52. Peak extraction using GSAS (LeBail method) gave an $R_{wp}$ value of 0.0556. The LeBail fit to the $Mo_4$PFT laboratory XRD pattern is shown in Figure 3.

**Figure 3:** LeBail fit to the laboratory X-ray powder diffraction data for [($^t$BuCO$_2$)$_3$Mo$_2$(μ-O$_2$CC$_6$F$_4$CO$_2$)Mo$_2$(O$_2$C$^t$Bu)$_3$]. Blue points represent the experimental diffraction pattern, the green line represents the refined fit to the pattern, the red line represents the difference curve, and the black ticks mark the expected peak positions.

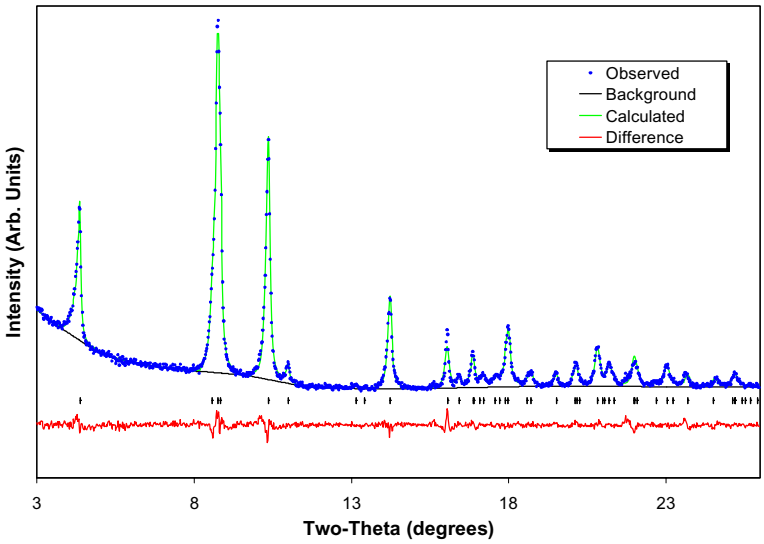


## ***4. Structure Determination***

Following the autoindexing and whole pattern fitting stages three possible space groups remained viable solutions for each compound. Each of these was investigated at the structure solution stage described below. In the case of $Mo_4$OXA, similar results were obtained using either the synchrotron or laboratory data. Analysis of the laboratory data is reported here. The molecular geometries were determined using density functional theory calculations as described in the main body of the paper. The structure determination was carried out using the global optimization approach implemented within DASH, the details of which are described elsewhere.[2]

*$Mo_4OXA$*

In the absence of special constraints associated with space group symmetry, the optimization process looks to obtain the best match to the experimental data by adjusting the following variables:

- 3 variables to describe the position of the molecule within the unit cell,
- 4 variables (quaternians[9]) to describe the orientation of the molecule,
- 6 torsional degrees of freedom associated with the *tert*-butyl group of each pivalate ligand,
- 1 torsional degree of freedom associated with a twist about the C-C bond of the oxalate group.

This reduces the number of variables from 156 (3 variables each for the 52 crystallographically distinct non-hydrogen atoms) to 14. In light of the relatively small number of observed reflections, this reduction in the number of variables is absolutely essential if one is to have any hope of extracting meaningful structural information from the powder patterns. In addition, certain space groups place additional constraints on the conformation or location of the molecule due to the symmetry elements present:

***$P2_1/a$*** $\rightarrow$ The center of gravity of each molecule must sit upon the inversion center. Consequently, there are no variables associated with the position of the molecule, and only three torsional degrees of freedom, as the left hand side of the molecule is related to the right-hand side by symmetry and the oxalate group is required by symmetry to be planar. (7 variables)

***Pa*** $\rightarrow$ The position of the molecule in the *ac* plane is arbitrary, only the distance from the glide plane is significant. (12 variables)

***$P2_1$*** $\rightarrow$ The position of the molecule along the *b*-axis is arbitrary, only the distance from the screw axes is significant. (13 variables)

The profile $\chi^2$ values given in Table 1 indicate the quality of fit that can be obtained from the DASH structural optimization using each model. These values show that a structure corresponding to unit cell **B** and space group *Pa* provides the best fit to the data. A model based upon unit cell B and space group $P2_1/a$ also provides a reasonable fit to the data. Models corresponding to space groups *C2* and $P2_1$ lead to solutions which are noticeably poorer. Coupled with the fact that the extinction conditions are not quite right for the *C2* solution, and the $P2_1$ solution produces a number of "accidental absences" these two possible solutions were discarded at this point. Our reasons for favoring the *Pa* solution over the $P2_1/a$ solution are explained in greater detail in the next section. **It is important to note that all four solutions produced structures which exhibit very similar molecular packing motifs. Since determination of the intermolecular connectivity is the main focus of our structural characterization efforts it should be realized that the principle conclusions of this work would be essentially the same regardless of choice of unit cell and space group.** The most significant difference among the four is that the bridging oxalate is constrained by symmetry to be planar in the $P2_1/n$ solutions, but not in the other solutions.

*$Mo_4PFT$*

In principle the degrees of freedom for the $Mo_4$PFT molecule are very similar to those described in the case of $Mo_4$OXA:

- 3 variables to describe the position of the molecule within the unit cell,
- 4 variables (quaternians[9]) to describe the orientation of the molecule,
- 6 torsional degrees of freedom associated with the *tert*-butyl group on each pivalate ligand,
- 2 torsional degrees of freedom associated with twists about the C-C bond of each carboxylate group extending from the phenyl ring.

This reduces the number of variables from 186 (3 variables each for the 62 crystallographically distinct non-hydrogen atoms) to 15. However, the restraints imposed by the space group symmetry are more numerous in this case. Regardless of the choice of space group, the

conformation of the molecule is no longer independent of symmetry. That is to say that not all atoms in the $Mo_4$PFT molecule are crystallographically unique ($Z' < 1$).

***C2*** → The two-fold axis must intersect the center of gravity of the molecule (the center of the aromatic ring), so that the two halves of the molecule are related by symmetry ($Z' = ½$). Since the y-coordinate of the molecule's position is arbitrary, there are no variables associated with the position of the molecule. By symmetry the aromatic ring should lie either parallel or perpendicular to the two fold axis so that only 1 variable is needed to specify the orientation of the molecule (a rotation about the *b*-axis). Finally, as the left hand side of the molecule is related to the right-hand side by symmetry there are only four torsional degrees of freedom. (5 variables)

***Cm*** → As the *b*-axis is only one molecule wide (along the shortest dimension of the molecule where no pivalate groups are extending out from the Mo-Mo multiple bond), the mirror plane must bisect the molecule. Thus the y-coordinate of the molecule is fixed, and its position in the xz-plane is arbitrary. This configuration also constrains the perfluoroterephtalate group (save the four oxygens), and three carbons from each pivalate group to lie on the mirror plane (molecular symmetry is $C_{2h}$). This leaves one variable to define the orientation of the molecule (a rotation about the *b*-axis) and two torsional degrees of freedom associated with the *tert*-butyl groups. (3 variables)

***C2/m*** → This space group combines the symmetry constraints of *C2* and *Cm*. The resulting rigid body refinement involves only one variable, which defines the orientation of the molecule. (1 variable)

As $Z' < 1$ for each of the above space groups, the structure optimization process for $Mo_4$PFT represents a somewhat non-standard application of DASH. In order to be strictly correct one should use a molecular fragment during the optimization process. However, in practice it was difficult to constrain the position of the molecular fragment to be in the proper location with respect to the respective symmetry operators. Therefore, the entire molecular was used during the optimization process. A correct solution can still be obtained if the molecule moves to a conformation where the symmetry operators map the molecule onto itself. In this case the overall scale factor can be varied to obtain appropriate occupancies. This was the behavior observed when the space group symmetry was taken to be *C2*, with the exception of 4 carbon and 4 fluorine atoms of the bridging perfluoroterephtalate group. The failure of these atoms to map onto each other is discussed in the next section. The DASH profile $\chi^2$ for the *C2* solution was a very respectable 5.82. As discussed above, when the space group symmetry was taken to be either *Cm* or *C2/m*, the torsion angles and molecular orientation had to be fixed so that the mirror plane bisects the Mo-Mo bond and contains the aromatic ring. Those constraints lead to a very unsatisfactory fit to the data, yielding a profile $\chi^2$ value of 84. Thus we can unambiguously discard the *Cm* and *C2/m* solutions and confirm that *C2* is the appropriate space group symmetry.

## ***5. Rietveld Refinement***

As a final step in the structure determination process rigid body Rietveld refinements were performed using the GSAS software suite,[8] with the initial position and orientation of the molecules being taken from the DASH output. Rigid body refinements were attempted and found to be stable, but did not lead to a noticeable improvement in the fit. Therefore, the atomic positions obtained from DASH were not refined. The background was modeled using a linear interpolation between manually selected, fixed background points. The variables that were

refined included the lattice parameters, a zero-point shift, peak shape parameters, a scale factor and a single isotropic displacement parameter.

Attempts were made to improve the fits by removing the rigid body constraints. These refinements were only stable if a large number of soft constraints were placed on the Mo-Mo, Mo-O, C-O, C-C, C-F and O-O distances, and these constraints were weighted very heavily. While this did lead to a significant improvement in the fit to the experimental patterns, it was not clear that more accurate pictures of the molecular conformations and packing were obtained. This behavior clearly shows that some distortions of the calculated gas phase molecular geometries are present in the solid state structures of both compounds, but unlike the pattern of molecular packing this information can not reliably be extracted from the powder diffraction patterns. The fact that the fit to the experimental data is better at low angles than at high angles is also consistent with this assessment.

*$Mo_4OXA$*

In contrast to the DASH analysis, in GSAS we were able to refine the synchrotron and laboratory X-ray patterns simultaneously. The final fits corresponding to the *$P2_1/a$* and *Pa* solutions are shown in Figures 4 and 5, respectively. The *Pa* solution is favored because it leads to a significantly better fit. Figure 6 shows the sensitivity of the refinement to changes in the torsion angle at the oxalate group. It is clear that the molecule is closer to planar at the oxalate group than it is to any other regular geometry, but it does not appear to be exactly planar. Tables 3 and 4 contain the details of the structure. The results are reported in the standard setting of the space group, *Pc*. Considering the highly constrained nature of this refinement, the complexity of the structure and the available data is not possible to unequivocally discard *$P2_1/a$* (*$P2_1/c$*) as a valid solution, but given the available information we feel that the structure is best represented by the *Pa* (*Pc*) model.

*$Mo_4PFT$*

As discussed at length in the previous section, the center of mass of the $Mo_4PFT$ molecule lies on a 2-fold rotation axis so that the two halves of the molecule are related by symmetry (Z′ = ½). Within the constraints of symmetry there are two possible ordered orientations of the planar aromatic ring, either parallel or perpendicular to the 2-fold axis. Alternatively, the plane of the $O_2CC_6F_4CO_2$ group could be disordered over two or more orientations. All three possibilities were evaluated during the final refinement stage. The disordered model provided a fit ($R_{wp}$ = 0.0796) to the experimental data far superior to models with the PFT group either parallel ($R_{wp}$ = 0.142) or perpendicular ($R_{wp}$ = 0.113) to the 2-fold axis. Additionally, the model with the aromatic ring parallel to the 2-fold axis leads to unrealistically short (~ 1 Å) F-F contacts. The final refinement results are contained in Tables 3 and 5, and the final fit to the data is shown in Figure 7.

## References


1 DASH was written by W.I.F. David and K. Shankland, and can be purchased from the Cambridge Crystallographic Data Centre, see www.ccdc.cam.ac.uk for more details.

2 W. I. F. David, K. Shankland and N. Shankland, *Chem. Commun. (Cambridge)*, 1998, 931.

3 A. Boultif and D. Louer, *J. Appl. Crystallogr.*, 1991, **24**, 987.

4 G. S. Smith and R. L. Snyder, *J. Appl. Crystallogr.*, 1979, **12**, 60.

5 P. E. Werner, L. Eriksson and M. Westdahl, *J. Appl. Crystallogr.*, 1985, **18**, 367.
6 G. S. Pawley, *J. Appl. Crystallogr.*, 1981, **14**, 357.
7 A. LeBail, H. Duroy and J. L. Fourquet, *Mater. Res. Bull.*, 1988, **23**, 447.
8 A. C. Larson and R. B. Von Dreele, 'GSAS Software Suite', Los Alamos, NM.
9 A. R. Leach, 'Molecular Modeling: Principles and Applications', 1996.

**Table 3:** Crystallographic data for $[(^tBuCO_2)_3Mo_2(\mu\text{-}X)Mo_2(O_2C^tBu)_3]$

| Formula | $[(^tBuCO_2)_3Mo_2(\mu\text{-}O_2C_2O_2)Mo_2(O_2C^tBu)_3]$ | $[(^tBuCO_2)_3Mo_2(\mu\text{-}O_2CC_6F_4CO_2)Mo_2(O_2C^tBu)_3]$ |
|---|---|---|
| Temperature/K | 295 | 295 |
| Formula Weight/g $mol^{-1}$ | 1007 | 1226 |
| Space Group | *Pc* | *C2* |
| a/Å | 16.045(2) | 21.011(3) |
| b/Å | 5.8170(6) | 5.7245(8) |
| c/Å | 26.817(2) | 20.586(3) |
| β/° | 118.826(7) | 101.307(7) |
| Volume/$Å^3$ | 2192.7(5) | 2427.8(7) |
| Z | 2 | 2 |
| Calculated Density/g $cm^{-3}$ | 1.51 | 1.68 |
| LeBail $R_{wp}$ (Lab Data) | 0.0708 | 0.0556 |
| Rietveld $R_{wp}$ (Lab Data) | 0.1056 | 0.0796 |
| LeBail $R_{wp}$ (Synch. Data) | 0.0445 | --- |
| Rietveld $R_{wp}$ (Synch. Data) | 0.1131 | --- |

**Table 4:** Fractional coordinates for $[(^tBuCO_2)_3Mo_2(\mu\text{-}O_2C_2O_2)Mo_2(O_2C^tBu)_3]$

| Atom | x | y | z | Occupancy |
|---|---|---|---|---|
| Mo1 | 0.74174 | 0.68817 | 0.55624 | 1 |
| Mo2 | 0.65146 | 0.40864 | 0.51235 | 1 |
| Mo3 | 0.34508 | 1.37937 | 0.47158 | 1 |
| Mo4 | 0.26196 | 1.0813 | 0.45996 | 1 |
| O1 | 0.74574 | 0.59121 | 0.63349 | 1 |
| O2 | 0.65031 | 0.29571 | 0.58707 | 1 |
| O3 | 0.86477 | 0.48722 | 0.5785 | 1 |
| O4 | 0.3818 | 1.39976 | 0.5586 | 1 |
| O5 | 0.29393 | 1.08462 | 0.54633 | 1 |
| O6 | 0.62524 | 0.90252 | 0.53673 | 1 |
| O7 | 0.76936 | 0.19153 | 0.53211 | 1 |
| O8 | 0.46656 | 1.18128 | 0.49266 | 1 |
| O9 | 0.52987 | 0.60733 | 0.49036 | 1 |
| O10 | 0.74438 | 0.7987 | 0.4818 | 1 |
| O11 | 0.37868 | 0.8665 | 0.48038 | 1 |
| O12 | 0.22699 | 1.59691 | 0.45089 | 1 |
| O13 | 0.13913 | 1.28163 | 0.43863 | 1 |
| O14 | 0.64892 | 0.50315 | 0.4354 | 1 |
| O15 | 0.31175 | 1.37843 | 0.38495 | 1 |
| O16 | 0.22384 | 1.0633 | 0.37264 | 1 |
| C1 | 0.80181 | 0.29754 | 0.73263 | 1 |
| C2 | 0.65448 | 0.52103 | 0.70658 | 1 |
| C3 | 0.69973 | 0.33738 | 0.68663 | 1 |
| C4 | 0.64309 | 0.11577 | 0.67669 | 1 |
| C5 | 0.47564 | 1.32323 | 0.67574 | 1 |
| C6 | 0.35563 | 1.02044 | 0.65893 | 1 |
| C7 | 0.30892 | 1.42929 | 0.64792 | 1 |
| C8 | 0.37204 | 1.25472 | 0.63954 | 1 |
| C9 | 0.97796 | 0.04356 | 0.63719 | 1 |
| C10 | 0.69847 | 0.41355 | 0.63181 | 1 |
| C11 | 0.34756 | 1.24564 | 0.57706 | 1 |
| C12 | 0.93793 | 0.12969 | 0.57639 | 1 |
| C13 | 1.01416 | 0.26657 | 0.57086 | 1 |
| C14 | 0.85117 | 0.28025 | 0.56126 | 1 |
| C15 | 0.91071 | -0.0752 | 0.53601 | 1 |
| C16 | 0.54271 | 0.81546 | 0.50745 | 1 |
| C17 | 0.45752 | 0.96342 | 0.49262 | 1 |
| C18 | 0.00412 | 1.54592 | 0.44922 | 1 |
| C19 | 0.09301 | 1.89189 | 0.44671 | 1 |
| C20 | 0.14891 | 1.49836 | 0.43881 | 1 |
| C21 | 0.69674 | 0.67994 | 0.43713 | 1 |
| C22 | 0.06217 | 1.64885 | 0.42367 | 1 |
| C23 | 0.79465 | 0.71152 | 0.38773 | 1 |
| C24 | 0.69699 | 0.75335 | 0.38257 | 1 |
| C25 | 0.6725 | 1.00732 | 0.37179 | 1 |
| C26 | 0.00059 | 1.66527 | 0.35919 | 1 |
| C27 | 0.25755 | 1.21836 | 0.35415 | 1 |
| C28 | 0.62449 | 0.61365 | 0.33211 | 1 |
| C29 | 0.2315 | 1.21204 | 0.2914 | 1 |
| C30 | 0.31725 | 1.28164 | 0.28513 | 1 |
| C31 | 0.20005 | 0.97057 | 0.26735 | 1 |

**Table 4:** Fractional coordinates for $[(^tBuCO_2)_3Mo_2(\mu\text{-}O_2CC_6F_4CO_2)Mo_2(O_2C^tBu)_3]$

| Atom | x | y | z | Occupancy |
|---|---|---|---|---|
| Mo1 | 0.6253 | 0.9503 | 0.2817 | 1 |
| Mo2 | 0.5825 | 0.6206 | 0.2541 | 1 |
| C1 | 0.4739 | 0.7680 | 0.5582 | 1 |
| C2 | 0.5207 | 0.6057 | 0.5487 | 0.5 |
| C3 | 0.5464 | 0.6091 | 0.4913 | 0.5 |
| C5 | 0.4791 | 0.9372 | 0.4515 | 0.5 |
| C6 | 0.4534 | 0.9338 | 0.5090 | 0.5 |
| C7 | 0.4463 | 0.7643 | 0.6200 | 1 |
| C8 | 0.6541 | 0.7922 | 0.1558 | 1 |
| C9 | 0.6824 | 0.7962 | 0.0927 | 1 |
| C10 | 0.7128 | 0.5693 | 0.3342 | 1 |
| C11 | 0.7739 | 0.4476 | 0.3718 | 1 |
| C12 | 0.4946 | 1.0017 | 0.2024 | 1 |
| C13 | 0.4331 | 0.1232 | 0.1659 | 1 |
| C14 | 0.4298 | 0.3694 | 0.1932 | 1 |
| C15 | 0.3729 | -0.0137 | 0.1748 | 1 |
| C16 | 0.4331 | 0.1365 | 0.0917 | 1 |
| C17 | 0.6405 | 0.6465 | 0.0397 | 1 |
| C18 | 0.7518 | 0.7014 | 0.1069 | 1 |
| C19 | 0.6845 | 0.0465 | 0.0671 | 1 |
| C20 | 0.7552 | 0.2689 | 0.4195 | 1 |
| C21 | 0.8205 | 0.6265 | 0.4107 | 1 |
| C22 | 0.8093 | 0.3246 | 0.3232 | 1 |
| F1 | 0.4084 | 1.0918 | 0.5169 | 0.5 |
| F2 | 0.5413 | 0.4443 | 0.5954 | 0.5 |
| F3 | 0.5914 | 0.4511 | 0.4834 | 0.5 |
| F4 | 0.4585 | 1.0986 | 0.4049 | 0.5 |
| O1 | 0.5873 | 0.9544 | 0.3699 | 1 |
| O2 | 0.5422 | 0.6060 | 0.3407 | 1 |
| O3 | 0.6656 | 0.9652 | 0.1952 | 1 |
| O4 | 0.6204 | 0.6164 | 0.1660 | 1 |
| O5 | 0.7114 | 0.7915 | 0.3341 | 1 |
| O6 | 0.6661 | 0.4426 | 0.3048 | 1 |
| O7 | 0.4962 | 0.7794 | 0.2022 | 1 |
| O8 | 0.5415 | 0.1285 | 0.2314 | 1 |

**Figure 4:** Fits to the laboratory (top panel) and synchrotron (lower panel) X-ray powder diffraction data for $[(^tBuCO_2)_3Mo_2(\mu\text{-}O_2C_2O_2)Mo_2(O_2C^tBu)_3]$, using the $P2_1/n$ solution. Simultaneous refinements of both data sets were carried out using the atomic coordinates from DASH as described in the text. Blue points represent the experimental diffraction pattern, the green line represents the refined fit to the pattern, the red line represents the difference curve, and the black ticks mark the expected peak positions.

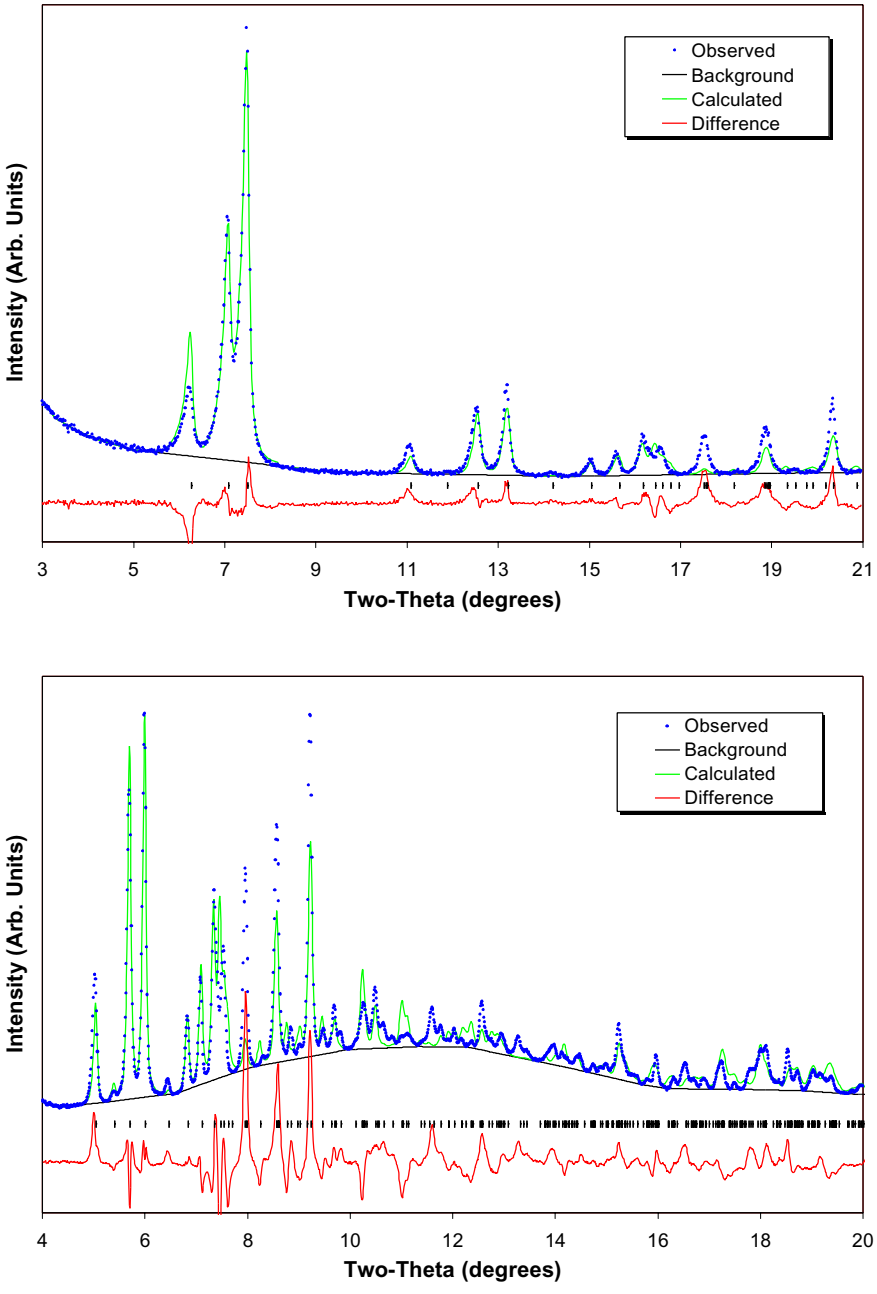

**Figure 5:** Fits to the laboratory (top panel) and synchrotron (lower panel) X-ray powder diffraction data for $[(^tBuCO_2)_3Mo_2(\mu\text{-}O_2C_2O_2)Mo_2(O_2C^tBu)_3]$, using the *Pc* solution. Simultaneous refinements of both data sets were carried out using the atomic coordinates from DASH as described in the text. Blue points represent the experimental diffraction pattern, the green line represents the refined fit to the pattern, the red line represents the difference curve, and the black ticks mark the expected peak positions.

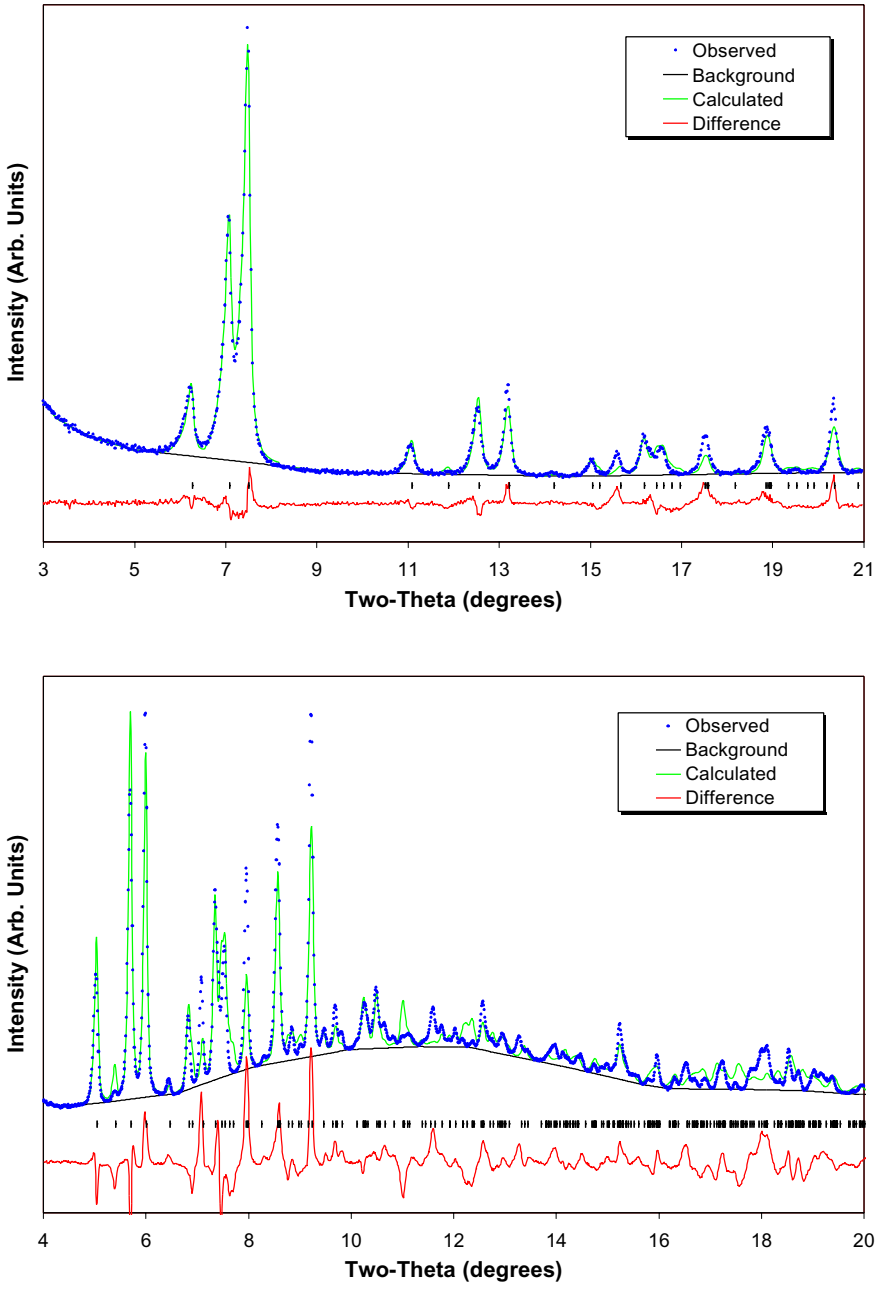

**Figure 6:** The sensitivity of the goodness of fit parameter, $R_{wp}$, to changes in the torsion angle at the oxalate group of $[(^tBuCO_2)_3Mo_2(\mu\text{-}O_2C_2O_2)Mo_2(O_2C^tBu)_3]$. The position of the molecule was allowed to refine at each step, while the conformation of the molecule (all torsions) were held fixed.

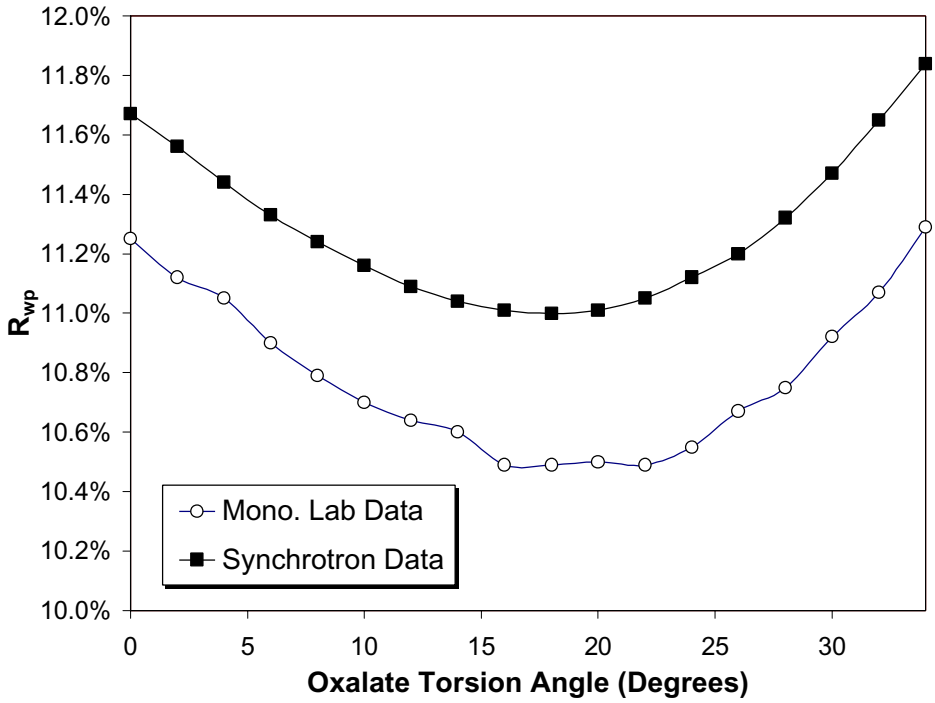


**Figure 7:** The fit to the laboratory X-ray powder diffraction data, using the *C2* solution for $[(^tBuCO_2)_3Mo_2(\mu\text{-}O_2CC_6F_4CO_2)Mo_2(O_2C^tBu)_3]$. Blue points represent the experimental diffraction pattern, the green line represents the refined fit to the pattern, the red line represents the difference curve, and the black ticks mark the expected peak positions.